Signature Modelling and Radiometric Rendering Equations in Infrared Scene Simulation Systems

Cornelius J. Willers[a], Maria S. Willers[b] and Fabian Lapierre[c]

[a] CSIR, P.O. Box 395, 0001 Pretoria, South Africa
[b] Denel Dynamics, P.O. Box 7412, 0046 Centurion, South Africa
[c] Rue Val de Mehaigne, 8/10, B-4520 Wanze, Belgium

ABSTRACT

The development and optimisation of modern infrared systems necessitates the use of simulation systems to create radiometrically realistic representations (e.g. images) of infrared scenes. Such simulation systems are used in signature prediction, the development of surveillance and missile sensors, signal/image processing algorithm development and aircraft self-protection countermeasure system development and evaluation.

Even the most cursory investigation reveals a multitude of factors affecting the infrared signatures of real-world objects. Factors such as spectral emissivity, spatial/volumetric radiance distribution, specular reflection, reflected direct sunlight, reflected ambient light, atmospheric degradation and more, all affect the presentation of an object's instantaneous signature. The signature is furthermore dynamically varying as a result of internal and external influences on the object, resulting from the heat balance comprising insolation, internal heat sources, aerodynamic heating (airborne objects), conduction, convection and radiation. In order to accurately render the object's signature in a computer simulation, the rendering equations must therefore account for all the elements of the signature.

In this overview paper, the signature models, rendering equations and application frameworks of three infrared simulation systems are reviewed and compared. The paper first considers the problem of infrared scene simulation in a framework for simulation validation. This approach provides concise definitions and a convenient context for considering signature models and subsequent computer implementation. The primary radiometric requirements for an infrared scene simulator are presented next.

The signature models and rendering equations implemented in OSMOSIS (Belgian Royal Military Academy), DIRSIG (Rochester Institute of Technology,) and OSSIM (CSIR & Denel Dynamics) are reviewed. In spite of these three simulation systems' different application focus areas, their underlying physics-based approach is similar. The commonalities and differences between the different systems are investigated, in the context of their somewhat different application areas.

The application of an infrared scene simulation system towards the development of imaging missiles and missile countermeasures are briefly described.

Flowing from the review of the available models and equations, recommendations are made to further enhance and improve the signature models and rendering equations in infrared scene simulators.

Keywords: infrared simulation, scene rendering, signature, SIG, DIRSIG, OSMOSIS, OSSIM

1. INTRODUCTION

Simulation is increasingly being used to support optical system development throughout all the product life-cycle phases, from concept analysis, system development to deployment and maintenance. The advent of imaging systems presented the need for simulation to provide accurate image rendering in the optical spectral ranges.[1–4]

Further author information: (Send correspondence to C.J.W.)
C.J.W.: E-mail: nwillers@csir.co.za, Telephone: +27-12-841-4261
M.S.W.: E-mail: riana.willers@deneldynamics.co.za, Telephone: +27-12-671-1901
F.L.: E-mail: f_lapierre@fastmail.fm, Telephone: +32 479 99 02 82

An accurate physics-based imaging simulation system can greatly assist in the development of optronic sensor systems. Modern sensor systems have complex sensor assemblies with performance depending on a variety of factors. Extensive use of modelling and simulation results in reduced risk, lower cost and shorter development time scales.[5,6] Detailed sub-system modelling and simulation can be used to (1) obtain insight and improve understanding; (2) support hardware development; (3) support design decisions; (4) develop and optimise algorithms; (5) evaluate test scenarios that are difficult to execute in real-life due to safety risk or cost considerations.

Accurate and comprehensive models of all observed objects (targets) and sensors (cameras) implement the behaviour of the real object in minute detail. Images created by these sensor models of detail and target-rich scenes are often indistinguishable from images created by real cameras of real scenes.

This paper, written from the OSSIM perspective, investigates the main characteristics of three such simulation systems. The three systems evolved from different origins but all share a common objective of calculating accurate renditions of an image of a scene containing objects of interest. This paper does not cover the Synthetic Image Generation (SIG) systems used in human observation training simulators.

The paper is structured to start with an overview of simulation validation in Section 2, followed by a brief description of the optical signatures and the requirements for rendering such signatures in Section 3. In Sections 4, 5 and 6 three simulation systems are briefly described. The information on the DIRSIG and OSMOSIS systems relayed here was obtained in open literature, while the information on the OSSIM system is first-hand from the developers. Section 7 provides some examples of the application of the OSSIM simulation system, while Section 8 concludes the paper.

2. IMAGE SIMULATION VALIDATION FRAMEWORK

2.1 Qualification, Verification and Validation

On the premise that a simulation is performed in lieu of real-world experiments, it is reasonable to expect that the simulation provides accurate results, relative to its intended real-world application domain. The model generally used for model verification and validation, as formally defined by the Society for Modelling and Simulation International (SCS),[7] as expanded,[8,9] recognises three distinct elements of the item under investigation: (1) the physical reality, (2) the conceptual model and (3) the simulation implementation. Figure 1 shows the relationships between the three elements.

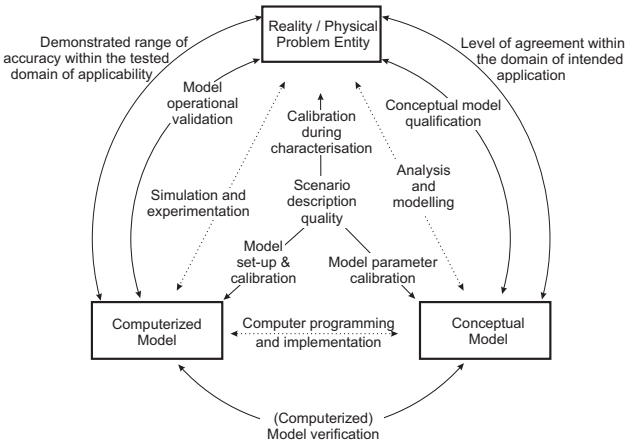

Figure 1. Summary of the Verification and Validation Process.[7,8]

The *Reality* is defined as "An entity, situation or system which has been selected for analysis."[7] The *Conceptual Model* is defined as "Verbal description, equations, governing relationships, or 'natural laws' that purport to describe Reality."[7] The *Computerized Model* is defined as "An operational computer program which implements the Conceptual Model."[7] Model *Qualification* is defined to mean "Determination of the adequacy of the Conceptual Model to provide an acceptable level of agreement for the domain of intended application."[7] Model *Verification* is defined to mean "Substantiation that a Computerized Model represents a Conceptual Model within the specified limits of accuracy."[7] Model *Validation* is defined as "Substantiation that a computerized model within its domain of applicability possesses a satisfactory range of accuracy consistent with the intended application of the model."[7]

Any Conceptual Model has a limited scope, expressed as the *Domain of Intended Operation*, which are the "Prescribed conditions for which the Conceptual Model is intended to match Reality."[7] Over the Domain of Intended Operation, there must be a known expected *Level of Agreement*, consistent with the purpose for which the model was built. Likewise, the Computerised Model will have a *Domain of Applicability*, where the "model

has been tested and compared against Reality",[7] with a demonstrated *Range of Accuracy*. Clearly, validation is only defined in terms of the application domain of the simulation, and nowhere else.

In the context of a complex scenario-based simulation, the accuracy of scenario descriptions are critical to the correct interpretation and/or execution of the model. Firstly, the scenario during a Reality measurement (e.g. infrared characterisation) must be accurately known and accounted for in the data reduction process. Secondly, the parameters in the Conceptual Model must be realistic in terms of real-world physical processes. Finally, the scenario parameters used to set up the Computerised Model must be applicable to the Reality scenario if Validation is sought.

2.2 Infrared Simulation Validation in Practice in OSSIM

2.2.1 Techniques for Verification and Validation

Verification and validation are generally done by a combination of objective (statistical or mathematical procedures) and subjective evaluations. A number of tests are described[8,10,11] which include (1) animation and operational graphics (e.g. images and videos), (2) comparison with other models, (3) parameter variation stress testing, (4) extreme condition testing, (5) expert opinion and Turing tests*, (6) comparison with historical evidence, (7) confirming internal consistency, (8) analysing parameter sensitivity, and (9) validating of predictions versus reality. Ideally, every model characteristic should be validated with a number of orthogonal techniques.

Verification as described above is generally done during the model development phase. However, once implemented, routine testing should be performed to confirm that the model implementation remains true to its original implementation. For this purpose, regression testing is used — testing against verified and trusted result vectors.

2.2.2 Procedure for Verification and Validation

Expanding on Sargent,[8] the following procedure is followed in verifying and validating the imaging infrared simulation models: (1) a simulation model specification is compiled, (2) objectives for accuracy are set, (3) the theories and assumptions underlying the model are extensively reviewed and tested, (4) the conceptual models are subjected to expert opinion, (5) throughout development, the model is extensively tested against reality observations and comparison with other models, (6) internal consistency checks and cross model consistency checks are performed, (7) extensive comparisons are made between simulation predictions and reality observations, (8) extensive and well documented scenario-based testing are used for regression testing and comparison with reality, (9) model reviews and upgrades are executed as new reality information becomes available.

3. RENDERING OF OPTICAL SIGNATURES

3.1 Optical Signatures

Accurate modelling of the scene requires calculation of the reflected, emitted and transmitted radiance components from all objects in the scene. Combining all these components ensures accuracy over the whole spectral range of operation; where reflected sun radiance dominates in the shorter wavelength regions and emitted radiance is more prominent in the longer wavelength bands. Some of the contributors to the optical signature are shown in Figures 2 and 3. The signature is affected by the optical properties of the object itself, but also by those of the surrounding objects. The atmosphere significantly affects the signature by attenuating the flux from the object and adding path radiance to the flux. Sections 4, 5 and 6 describe three software systems used to render objects' signatures in the form of an image. The images thus rendered are used in a variety of different applications.

*The Turing test was originally defined to test whether a noninteractive human operator can distinguish between a computer performing a task versus a human performing the same task. We extend this notion to the test as to whether a user or other application can discriminate between the output of the simulation and reality.

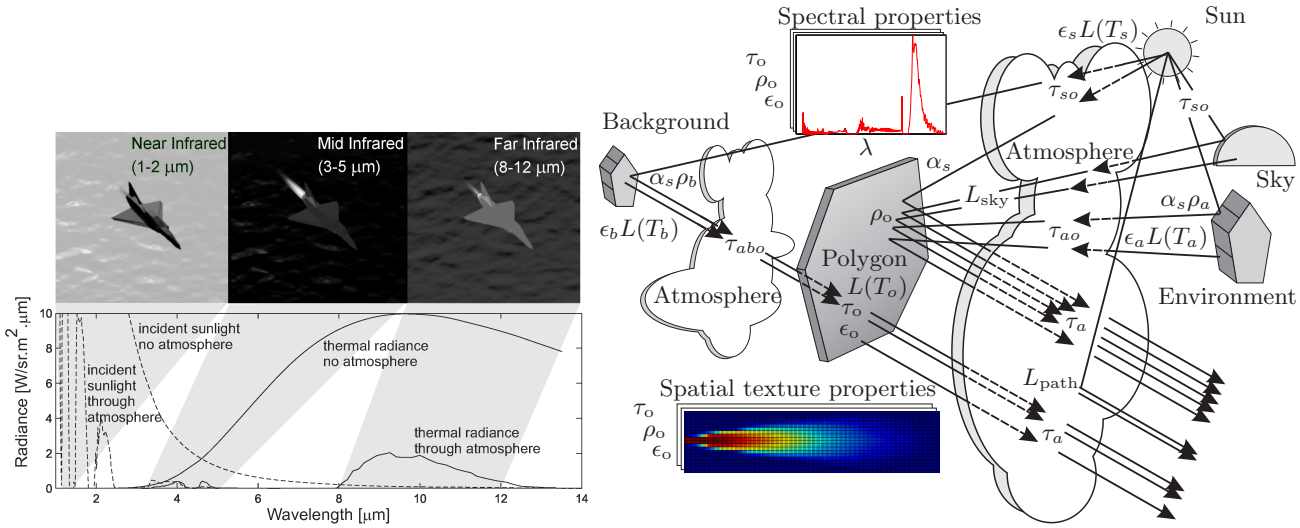

Figure 2. Main contributors to the OSSIM radiometric signature (variables defined in Table 1).[12]

3.2 Summary Requirements For Signature Rendering

Signature rendering systems generally form part of a larger application system. The key requirements for such a simulation system are (1) radiometric accuracy using physics-based, spectral radiometric floating point image calculation, typically covering the spectral range 0.4–20 μm, (2) accurate target signatures, including self-emitted flux and reflected and/or transmitted sunlight, ambient and sky radiance (i.e. all the components shown in Figure 2), (3) accurate spectral atmospheric path radiance and transmittance, (4) support for a variety of different and adverse environmental conditions, (5) accurate system models (sensor, signal processing, gimbals, missile aerodynamics and flight behaviour) and (6) a full three-dimensional world, where objects can move in all six degrees of freedom: remain stationary, move on the terrain or fly through space.

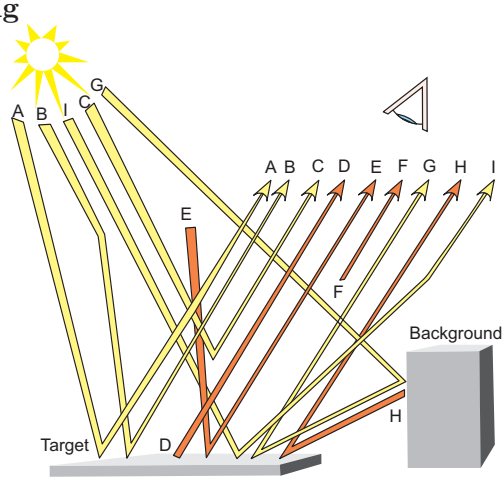

Figure 3. DIRSIG signature radiance components.[13]

4. THE DIRSIG SIMULATION SYSTEM

4.1 Introduction

"The Digital Imaging and Remote Sensing Image Generation (DIRSIG) model is a first principles based synthetic image generation model developed by the Digital Imaging and Remote Sensing Laboratory at Rochester Institute of Technology."[1]

"The DIRSIG model is a complex synthetic image generation application which produces simulated imagery in the visible through thermal infrared regions. The model is designed to produce broad-band, multi-spectral and hyper-spectral imagery through the integration of a suite of first principles based radiation propagation submodels. These submodels are responsible for tasks ranging from the bi-directional reflectance distribution function (BRDF) predictions of a surface to the dynamic scanning geometry of a line scanning imaging instrument. All modeled components are combined using a spectral representation and integrated radiance images can be simultaneously produced for an arbitrary number of user defined bandpasses."[14]

4.2 Application Areas

Early DIRSIG development was originally driven from remote sensing needs, but its developers' and sponsors' needs required a flexible and modular approach, supporting applications and technologies in areas such as Light

Table 1. Terminology definition for object signatures in OSSIM and OSMOSIS.

Symbol	Meaning	Symbol	Meaning
$L_{\Delta\lambda}$	total radiance in the wavelength band $\Delta\lambda$	n_r	object wideband index of refraction
$L(T_s)$	spectral black body radiance, sun temperature T_s	n	specular exponent
$L(T_a)$	spectral black body radiance, environment temperature T_a	τ_o	object surface spectral transmittance
$L(T_b)$	spectral black body radiance, background temperature T_b	τ_a	object to sensor spectral atmospheric transmittance
$L(T_o)$	spectral black body radiance, object temperature T_o	τ_{abo}	background to object spectral atmospheric transmittance
L_{path}	spectral atmospheric path radiance: emitted & scattered	τ_{ao}	ambient to object spectral atmospheric transmittance
L_{sky}	spectral sky radiance: emitted & scattered	τ_{so}	sun to object spectral atmospheric transmittance
ϵ_s	solar surface's spectral emissivity	Δ_τ	spatial texture variation in transmittance
ϵ_a	ambient environment's spectral emissivity	α_s	$A_{\text{sun}}/(d_{\text{sun}}^2\pi) = 2.17 \times 10^{-5}$
ϵ_b	background spectral emissivity	A_{sun}	area of the sun
ϵ_o	object surface spectral emissivity	d_{sun}	distance to the sun
Δ_ϵ	spatial texture variation in emissivity	θ_a	angle between the surface normal and the vertical
ρ_o	object surface spectral diffuse reflectance	θ_s	angle between the surface normal and solar incidence
ρ_s	object wideband Fresnel reflection	θ_r	angle between the reflected sunlight ray and the viewing direction
Δ_ρ	spatial texture variation in reflectivity	$\mathcal{S}$	camera spectral response

Detection and Ranging (LIDAR), RADAR, cloud modelling, low-light level, photon mapping, hyper-spectral imaging, multimodal sensor fusion and polarimetric imaging. DIRSIG is used in a very wide range of applications including sensor modelling and optimisation,[15] algorithm development (training and testing) and as an analysis aid.

4.3 Models and Equations

The DIRSIG rendering equation is widely referred to as the *Big Equation*,[13,16] alluding to the completeness of the equation as a signature radiometry model. The DIRSIG documentation employs the graphic shown in Figure 3 to denote the various components of the rendering equation. The L_I component is often combined with the L_C component,[16] as is also done here. The rendering equation is then stated as follows:

$$L_\lambda = \tau_{2\lambda}\left\{\overbrace{\underbrace{\frac{E'_{s\lambda}}{\pi}\tau_{1\lambda}r_\lambda\cos\sigma}_{\text{reflected sunshine}}}^{\text{A}} + \overbrace{\underbrace{\epsilon_\lambda L_{T\lambda}}_{\text{thermally emitted}}}^{\text{D}} + \underbrace{r_{d\lambda}F\left[\overbrace{\frac{E_{ds\lambda}}{\pi}}^{\text{B}} + \overbrace{\frac{E_{d\epsilon\lambda}}{\pi}}^{\text{E}}\right]}_{\text{reflected sky}} + \underbrace{r_{d\lambda}(1-F)\left[\overbrace{L_{bs\lambda}}^{\text{G}} + \overbrace{L_{b\epsilon\lambda}}^{\text{H}}\right]}_{\text{reflected background}}\right\} + \underbrace{\overbrace{L_{us\lambda}}^{\text{C}} + \overbrace{L_{u\epsilon\lambda}}^{\text{F}}}_{\text{atmospheric path radiance}}, \quad (1)$$

where L_λ is the spectral radiance at the entrance pupil of the sensor, $\frac{E'_{s\lambda}}{\pi}$ is the exo-atmospheric radiance onto a surface perpendicular to the incident sun light, $\tau_{1\lambda}$ is the atmospheric transmission coefficient along the sun-target path, $\cos\sigma$ accounts for the off-axis angle between the sun and the target normal, r_λ is the target reflectance, ϵ_λ is the target emissivity, $L_{T\lambda}$ is the Planck law thermal radiation from an object at temperature T, F is the fraction of the hemisphere above the target that is filled by the sky, $\frac{E_{ds\lambda}}{\pi}$ atmospheric downwelled solar irradiance, expressed as surface radiance on the target, $\frac{E_{d\epsilon\lambda}}{\pi}$ atmospheric downwelled self-emitted irradiance, expressed as surface radiance on the target, $r_{d\lambda}$ is the target diffuse reflectance, $L_{bs\lambda}$ is the background reflected solar radiance onto the target, $L_{b\epsilon\lambda}$ is the background reflected self-emitted radiance onto the target, $\tau_{2\lambda}$ is the atmospheric transmittance along the target-sensor path, $L_{us\lambda}$ the path radiance due to scattered sunlight and

$L_{u\epsilon\lambda}$ the path radiance due to atmospheric self-emittance. For comparison with the rendering equations in the following sections, Equation 1 is appropriately labelled.

DIRSIG employs a forward-chaining differential thermodynamic model to calculate the temperatures of background objects in the scene. The model includes[14,17,18] heat conduction into the bulk of the material (but not lateral conduction to adjacent facets), heat transfer by convection, diffuse sky irradiance, heat transfer by radiation and absorbed solar energy. The calculation of solar absorption accounts for sun shadow history, including partial obscuration by transmissive objects and clouds. Allowance is made for thermal shadow calculation on a level smaller than the size of the facet, in order to achieve realistic results in the vicinity of the shadow.

4.4 Implementation Summary

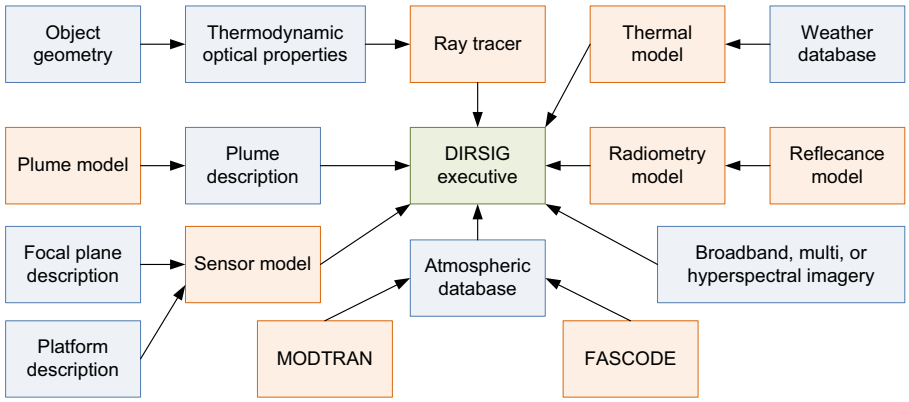

Figure 4. DIRSIG submodel interactions.[16]

DIRSIG comprises a set of submodels, each performing a specialised task, as shown in Figure 4.

DIRSIG uses a non-uniform subdivision (octree) ray tracing algorithm to determine which facets contribute radiance to each pixel in a synthetic image. The ray tracer accounts for opaque and transmissive facets. It also accounts for limited multibounce to account for interactions between facets within a scene. Transmission losses are taken into account when tracing all of the rays.[19]

DIRSIG uses a MODTRAN-based look-up table generator to correct for atmospheric effects. To support accurate hyper-spectral algorithm development, a full hemisphere sky map is used in a rigorous calculation when directly viewing the sky and for BRDF determination of the radiance reflected by a scene element.[14]

DIRSIG employs a mapping system to support material attributes at a resolution smaller than individual facets or polygons in an object. The map, similar to a texture map drawn over the facet, provides a pixel value, which is used as an index to identify material properties *at pixel level*. Photo interpretation of class type from thermodynamic databases, are used for the assignment of thermal materials property classes in texture maps.

To support development and understanding of the rendering process, DIRSIG supports per-pixel *truth maps*. These truth maps report on image pixel level, a number of intermediate results, including material class, shadow maps, sky exposure maps, ray trace hit maps, various sources' radiance maps, surface reflectance, surface temperature, atmospheric transmission, and plume maps.

4.5 Validation

DIRSIG and submodels are validated as reported.[20]

5. THE OSMOSIS/SAFIR SIMULATION

5.1 Introduction

OSMOSIS[21] calculates the infrared signature of a naval vessel by solving a heat balance equation to calculate the temperatures on the surface of the vessel. OSMOSIS employs the SAFIR[22] image rendering software to compute the infrared image. However, as part of the temperature calculation, OSMOSIS uses infrared calculations similar to those used in infrared image rendering.[23]

While OSMOSIS is focussed on the calculation of maritime vessel hull temperatures, SAFIR is a general purpose infrared rendering software,[24] with the aim of photo-realistic rendering of three-dimensional scenes. SAFIR produces physically-based synthetic imagery for land, air and naval scenarios, in the spectral band 0.3–25 μm. The modular structure of SAFIR supports its flexible application with diverse application software modules. In this section the focus falls on its application with OSMOSIS.

5.2 Application Areas

OSMOSIS is strongly focussed on the maritime environment, with scenarios comprising maritime vessels, the sea surface and blue sky. The vessel signature is calculated using a heat balance equation. The images are rendered in SAFIR.[22]

5.3 Models and Equations

The SAFIR rendering equation,[22] used to calculate scene radiance, can be summarised as shown in Equation 2. The terminology and symbols are defined in Table 1. The original reference[22] used a term L_{refrac} which is not defined and given the context, is interpreted and reported here, with hesitation, as a transmitted background radiance.

$$L_{\Delta\lambda} = \overbrace{\int_\lambda \epsilon_o L(T_o)\tau_a \mathcal{S} d\lambda}^{\text{thermally emitted}} + \overbrace{\int_\lambda L_{\text{path}} \mathcal{S} d\lambda}^{\text{atmospheric path radiance}} + \overbrace{\int_\lambda \epsilon_b L(T_b)\tau_{abo}\tau_o\tau_a \mathcal{S} d\lambda}^{\text{transmitted background}} + \overbrace{\int_\lambda \int_{2\pi} BRDF\left(L_{\text{sun}} + L_{\text{sky}} + L_{\text{env}}\right)\tau_a d\Omega d\lambda}^{\text{reflected radiance}}. \quad (2)$$

In order to calculate the scene radiance, SAFIR employs a three-dimensional description of all objects in the scene, object material properties, object surface temperature, meteorological conditions and the objects' movement in the scenario. The dynamic sea surface is modelled as a pre-calculated data set of temporal samples. Each temporal sample is calculated as the sum of multiple spatially-scaled two-dimensional Perlin noise fields.

Sea surface radiance is calculated for both self-emittance and reflected sun and ambient light. The Fresnel reflection equation is used to calculate reflectance ρ and, from reflectance, the emissivity in the infrared is calculated as $\epsilon = 1 - \rho$ (assuming water $\tau \to 0$). SAFIR also calculates sun glint on the sea surface. The Monte Carlo ray tracing technique used by SAFIR calculates the reflectance between surfaces, thereby creating vessel reflections from the sea surface. Sun glint on the sea surface is modelled by a BRDF model.

SAFIR employs MATISSE[25] to calculate spectral atmospheric transmittance and path radiance and a marine boundary layer module to calculate the refraction and other atmospheric effects present in the maritime environment.

The SAFIR sensor model includes the effect of sensor spectral response, optics modulation transfer function (MTF), detector MTF and various detector noise sources and charge transfer efficiency.

Core to OSMOSIS is the calculation of object temperatures, using the architecture shown in Figure 5. Defining heat flow to/from an object as positive/negative, and assuming short term steady state, an object's internal temperature is found as the solution of the detailed OSMOSIS heat balance equation[21]

$$Q_a + Q_{\text{sky}} + Q_{\text{env}} + Q_t + Q_k + Q_d = Q_{net} \to 0, \quad (3)$$

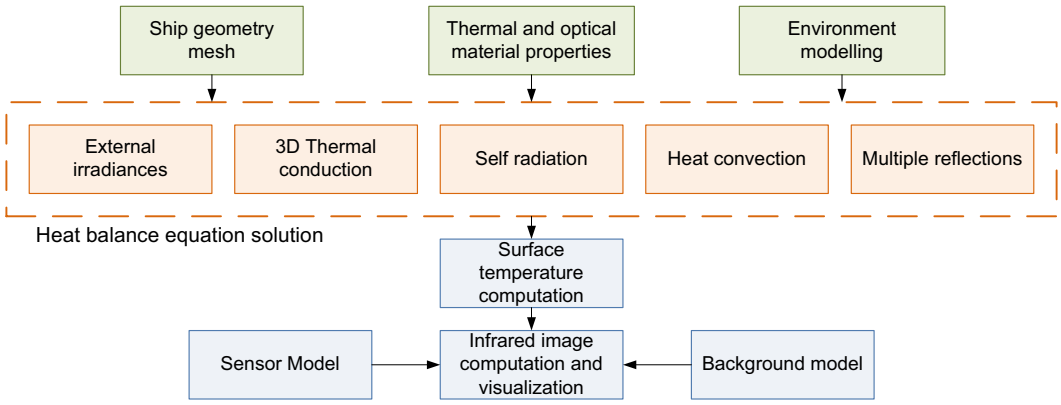

Figure 5. General architecture of OSMOSIS.

where Q_a is the absorbed solar energy, Q_{sky} is the energy absorbed from sky, Q_{env} is the energy absorbed from the sea or terrain environment, Q_t is the radiated energy, Q_k is the energy transferred by convection, $Q_d = C_h g p \frac{dT_{in}}{dt}$ conduction between the surface and internal heat source (intra object heat flow), C_h is the specific heat capacity, $g = 2h$ is the effective penetration depth of heat flow and p is the density of the object.

Heat conduction into the material is modelled, but not heat conduction between adjacent, touching materials. An object facet is assumed to consist of more than one material layer, hence T_{in} is a function of depth into the object.

An object facet can only absorb solar energy if the line of sight between the facet and the sun is unobstructed, thereby accounting for shadow effects when calculating object temperatures. Shadows of arbitrary complex shapes can be calculated, using an optimised algorithm to save computation time. OSMOSIS runs at near real-time speeds.

OSMOSIS handles parametric emissivity, i.e., the emissivity is a function of the wavelength, of object temperature, and of the angle of arrival of the optical beam on the object surface.

5.4 Implementation Summary

OSMOSIS is written in the Python[26] language. OSMOSIS can be readily integrated into other software by using SWIG[27] to expose a C/C++ interface to the Python modules.

5.5 Validation

OSMOSIS has been validated[28] against CUBI[29] measurements and calculations with RadThermIR.[2] For the validation by measurement, a CUBI test target was constructed, instrumented and the surface temperatures measured. The validation process indicated that it is important to use appropriately different emissivity values for short wave solar absorption and long wave emission — if possible, it is best that spectral emissivity be used. Ground radiance, multiple reflections and lateral thermal conduction do affect the predictions. It was found that the thermal conduction into the depth of the material has a significant effect on accuracy. The effect of sky irradiance was found to be small (compared to other sources). Finally it was found that under clear sky, warm ambient conditions, the effect of lateral (inter-facet) conduction has a significant effect on accuracy.

OSMOSIS has also been partially validated against data recorded onboard the Quest vessel during the SAPPHIRE trial conducted in 2006 in Chesapeake Bay.[21]

6. THE OSSIM SIMULATION SYSTEM

6.1 Introduction

The Optronic Scene Simulator (OSSIM) is a second-generation scene simulator† that creates synthetic images of arbitrary complex scenes in the visual and infrared (IR) bands, covering the 0.4–20 μm spectral region. These images are radiometrically accurate and based on theoretical physics models.

OSSIM[12] is developed as a collaborative effort between the CSIR and Denel, following a strategy of joint development of shared core infrastructure capability, but private development of application modules at the user level. This highly modular and decoupled approach means that OSSIM is readily adapted to new, previously unconsidered, applications.

6.2 Application Areas

The primary use for OSSIM include development, optimisation and performance prediction in the areas of (1) missile seeker sensors and thermal imager systems, (2) signal and image processing algorithms, (3) sensor algorithms, and (4) missile seeker countermeasures (Directed Infrared Countermeasure (DIRCM) simulator development is currently underway). OSSIM is also used for (1) flight test preparation, (2) Hardware in the Loop Simulation (HILS) for small images at real-time speeds, and (3) research in infrared signature modelling.

Various aircraft, missiles and other airborne, sea-based and ground-bound objects and countermeasures are viewed against clear sky, overcast sky and terrain and sea clutter backgrounds. The system creates radiometrically accurate images in any number of spectral bands simultaneously. The system supports two modes: open-loop (missile response does not affect missile location in the scene) and closed loop (missile response determines its position in the scene).

6.3 Models and Equations

The geometrical shape of objects and the terrain topography is described in terms of a three-dimensional complex hull, consisting of a set of flat, convex facets or polygons. Each polygon is assigned spectral radiometric properties, temporally variable spatial texture properties and radiometric properties. Polygons can also be partially transparent to represent gas clouds, countermeasure flares or aircraft plumes. True volumetric modelling is currently in development. The main contributors to signature radiance are shown in Equation 4, where the variables are defined in Table 1 and Figure 2.

$$
\begin{aligned}
L_{\Delta\lambda} \;=\; & \overbrace{\Delta_\epsilon \int_\lambda \epsilon_o L(T_o)\tau_a \mathcal{S} d\lambda}^{\text{thermally emitted}} \;+\; \overbrace{\int_\lambda L_{\text{path}} \mathcal{S} d\lambda}^{\text{atmospheric path radiance}} \;+\; \overbrace{\Delta_\tau \int_\lambda \epsilon_b L(T_b)\tau_{abo}\tau_o\tau_a \mathcal{S} d\lambda}^{\text{transmitted background}} \\
& + \Delta_\rho \left[\overbrace{\int_\lambda \int_{\text{env}} \epsilon_a L(T_a)\tau_{ao}\rho_o\tau_a \mathcal{S} d\Omega d\lambda}^{\text{reflected background}} \;+\; \overbrace{\cos\theta_a \int_\lambda \int_{\text{sky}} L_{\text{sky}}\rho_o\tau_a \mathcal{S} d\Omega d\lambda}^{\text{reflected sky}} \right. \\
& \left. + \overbrace{\alpha_s \cos\theta_s \int_\lambda \epsilon_s L(T_s)\tau_{so}\rho_o\tau_a \mathcal{S} d\lambda}^{\text{diffuse reflected sunshine}} \;+\; \overbrace{\left[\frac{\alpha_s(n+1)\rho_s \cos^n\theta_r}{2}\right] \int_\lambda \epsilon_s L(T_s)\tau_{so}\tau_a \mathcal{S} d\lambda}^{\text{specular reflected sunshine}} \right] . \qquad (4)
\end{aligned}
$$

As indicated in Equation 4, all calculations are spectral calculations to account for the spectral nature of some sources (e.g. CO_2 plumes). In the trivial case of constant emissivity, such calculations are made once at the start of the simulation. For spectrally varying sources, the spectral formulation, including a spectral atmospheric transmittance, is evaluated for every image frame.

To allow for the subtleties and full scope of variability in atmospheric attenuation, the simulation employs all capabilities of the MODTRAN[30] computer code. Using MODTRAN's Joint Modelling and Simulation Systems

†OSSIM, in development since 2004, is based on the first generation Simulation for Infrared System (SIMIS), developed within Denel since 1990. OSSIM is a complete rewrite in advanced C++ technologies.

(JMASS) interface, MODTRAN is directly linked into the simulation software. The user sets up the appropriate atmospheric conditions, whereafter the simulation sets up the path geometry as required and executes MODTRAN. After completion of the run, the simulation incorporates the MODTRAN results in its internal spectral radiometric calculations. MODTRAN can be invoked for every image frame or appropriately pre-computed MODTRAN tables can be loaded.

Object and terrain radiative temperature is calculated with a heat balance equation.[31–34] Terrain thematic maps are constructed by photo-interpretation of remote sensing images. These thematic maps identify material types used for diurnal temperature measurements. Defining heat flow in/out of the objects as positive/negative, and assuming short term steady state, the object internal temperature T_{in} is found as the solution of

$$Q_a + Q_e + Q_t + Q_k + Q_v + Q_i + Q_d = Q_{net} \to 0, \tag{5}$$

where Q_a is the absorbed solar energy, Q_e is the absorbed energy from the terrain and sky, Q_t is the radiated energy, Q_k is the energy transfer by convection, Q_v is the energy loss by evaporation, Q_i represents internal heat sources and aerodynamic heating,[31] and $Q_d = C_h g p \frac{dT_{in}}{dt}$ is the conduction into the object. C_h is the specific heat capacity, $g = 2h$ is the effective penetration depth of heat flow and p is the density of the object.

Most of the OSSIM applications thus far did not critically require shadows in either the thermal dynamics or image rendering calculations. Since OSSIM's scope is expanding, shadow capability will be added in future.

6.4 Implementation Summary

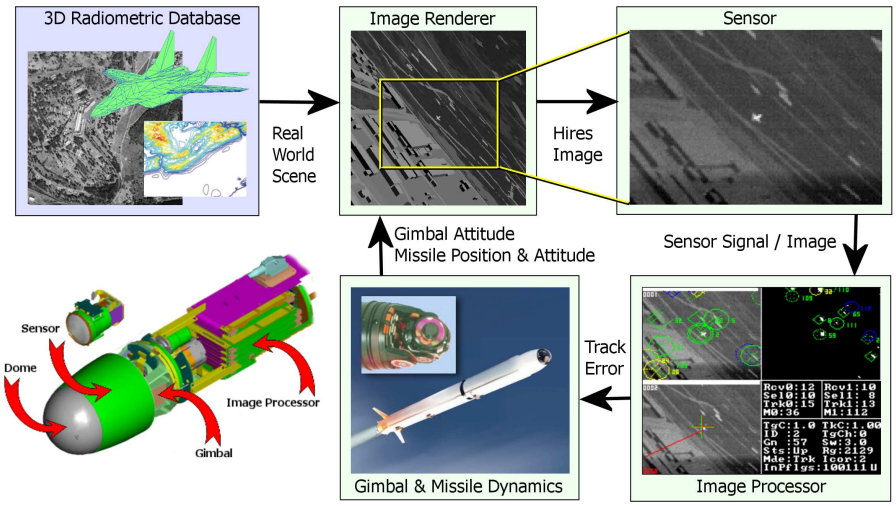

Figure 6. Infrared missile closed loop simulation model components.

The simulator has a modular approach with a standard core — radiometry calculation, image renderers, time management and similar functions — with well-defined interfaces to support a variety of specialist user subsystem models. These user modules mimic the real-world hardware in operation, degradation and performance. The image renderer extracts the three-dimensional scene data from the database and renders two-dimensional ideal 'high resolution' images simultaneously in multiple spectral bands. These images are computed at a higher resolution than the camera resolution, for subsequent sensor image calculation at a lower resolution. The specialist user application modules now process the rendered high resolution image to create the sensor image. For an infrared missile (Figure 6), the user modules consist of models describing the various sub-systems: the sensor sub-assembly, the image processing, the mechanical gimbal, as well as the missile dynamics and kinematics.

The *sensor sub-assembly module* models the sensor hardware system, typically accounting for the field of view, optical vignetting and point spread function (PSF), mechanical image scanning, detector type, detector

noise and focal plane processing, electronics signal transfer functions, as well as processing time delays. The sensor image so obtained is indistinguishable from a real camera image.

The *image processor module* processes the detector signal or image to determine the error signal for the purpose of target designation and tracking. Typical processing includes detection algorithms, automatic target recognition algorithms, auto-tracking algorithms, counter-countermeasure algorithms and control algorithms.

In a missile, the *gimbal* stabilises the sensor sight-line against missile vibration and base motion. The gimbal module describes the gimbal mechanical properties, inertial and mechanical angular sensors, sensor platform dynamics and kinematics and the stabilisation and tracking control systems. The tracking system keeps the target in the centre of the sensor field of view and provides the target sight-line rate as output.

The *missile module* uses the target sight-line rate to determine a guidance command and adjust the missile location and attitude in the world accordingly. The module comprises models for the missile aerodynamics, flight control servos, the auto-pilot, guidance and navigation.

The simulation is written in the C++ object oriented language, resulting in a modular and extendable software code base. The architecture provides a strong decoupling between 'user code' and simulation core library code. Strict software engineering discipline is applied to ensure low life cycle cost and long term maintainability.

Objects in the scene all fit in a class hierarchy of increasingly more specialised objects. The base class is *World Objects* which represent all objects in the world. Some objects have the additional property of movement (*Moving Objects*), while some objects have more specialised properties of observation (*Observer Objects*). This hierarchy ensures that all objects are visible in the world, and hence that all observer objects can observe any and all other objects in the world. The simulation supports an arbitrary number of movings and observers. For example, an optical missile warning sensor and an approaching missile can observe each other throughout the engagement.

OSSIM uses a finite difference equation library to model control systems, flight dynamics and kinematic movement. If required, OSSIM can also interface to Matlab as a mex function.

Although not developed for this purpose, OSSIM is currently deployed in a real-time HILS system with demonstrated performance of 25 Hz for an image size of 256×256, for a scene of 350 polygons.

6.5 Validation

Following the principles outlined in Section 2, the OSSIM core library and user modules are continually validated. An integrated procedure of infrared signature measurement, data analysis and conceptual modelling ensures that the conceptual models reasonably represent reality (i.e. qualified). The computer model implementations are rigorously tested in once-off verification tests and subsequent regression tests. Finally, the simulation outcomes are compared with, and corrected against, the reality observations during field trials (i.e. validated).

7. APPLICATIONS IN MISSILE AND COUNTERMEASURE DEVELOPMENT

7.1 Infrared Scene Simulation in Imaging Missile Development

OSSIM, and its predecessor SIMIS, proved to be invaluable in the development of advanced electro-optical sensor systems within Denel. The complexities of modern imaging systems demand a comprehensive simulation environment where the interplay between sensor, environment and target can be modelled, studied and evaluated under diverse environmental conditions and varied scenarios. The simulation is the *only* means to evaluate system performance for scenarios that cannot be executed in field trails, due to safety or cost considerations. The sensor simulation is used in parallel with hardware development to improve on understanding and to support problem solving. Extensive use of this simulation has consistently resulted in reduced risk, lower cost, and shorter development time scales. Examples of imaging missile seeker development within the simulation environment are discussed in this section.

The sensor model converts the rendered high resolution image into a sensor image, accounting for the sensor hardware imager artifacts. The objective is to calculate an image in the simulation that will look exactly like the real-world sensor image. This model simulates the optical system, detector and focal plane processor and initial

signal processing. The simulation supports the modelling of various sensor types, e.g reticle scanners, scanning linear array detectors, or staring array sensors. The sensor model output signal or image serves as input to the missile image processor.

Imaging sensors containing mechanical scanners normally comprise oscillating or rotating optical elements. Image formation is achieved by synchronising the mechanical movement of the scanner, modelled in the simulation by changing the instantaneous viewing angle, with signal sampling in the electronics. Accurate spatial position calculation is required to model the stretching and contraction of a fast-moving target when along-scanned by an oscillating mirror, as illustrated in Figure 7.

The detector geometrical, noise and electro-optical parameters serve as input to the simulation to obtain an accurate conversion from optical flux to signal or image values. The detector current is calculated as

$$\mathrm{I_{Detector}} = \Phi_{\mathrm{Detector}} \mathcal{R} \Delta\mathcal{R} + \mathrm{I_{Leakage}}, \tag{6}$$

where Φ_{Detector} is the total incoming flux, $\mathcal{R}$ the detector responsivity, $\Delta\mathcal{R}$ the detector non-uniformity (statistical tolerance variation for the different detector elements) and $\mathrm{I_{Leakage}}$ the detector leakage current. The optical flux on the detector is given by

$$\Phi_{\mathrm{Detector}} = \Phi_{\mathrm{Scene}} \otimes \mathrm{PSF} + \Phi_{\mathrm{Optics}} + \Phi_{\mathrm{Optics\ Mounting}} + \Phi_{\mathrm{Heated\ Air}} + \Phi_{\mathrm{Heated\ Dome}}. \tag{7}$$

Included in this equation are flux due to the scene contents (including the atmosphere) convolved with the PSF, flux from the heated optics and optics mountings, as well as flux contribution from the hot dome and hot air in front of the dome.

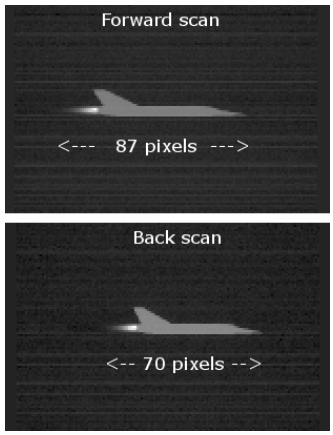

Figure 7. Stretching and contraction of a fast-moving target.

All theoretical noise sources are modelled. The detector shot noise varies with the square of the detector current and therefore increases with the sensor internal temperature and dome temperature. Electronic thermal and shot noise contributions, as well as non-theoretical noise sources as measured on the sensor hardware, e.g. $1/f$ noise and interference signals, are also modelled.

The highly detailed sensor electronics model accurately represents the signal transfer, including component tolerance variations in component parameters, amplifier gains and offsets, filter effects, saturation limits, and component noise. The digital signal processing module of the sensor model includes signal noise estimation and dynamic range analysis, non-uniformity correction (NUC), sensor automatic gain control (AGC) and background current subtraction (DCS) algorithms.

7.1.1 Sensor Algorithm Development

Modern infrared sensors employ intricate control and correction algorithms to achieve the required performance. During the recent development of an air-to-air imaging missile, the sensor NUC, DCS and AGC algorithms were developed and evaluated in the simulation environment, even before the first hardware was completed or tested. Figure 8 demonstrates the operation of the NUC and DCS correction algorithms for a linear vector scanned imager. To ensure optimal and effective algorithm development, the sensor model has to accurately account for minute details in the design and implementation. Hardware evaluation tests, simulation model updates and subsequent algorithm optimisation usually follow a continual cycle throughout development.

7.1.2 Sensor Hardware Development Support

A significant advantage of the detailed sensor simulation model is that signals deep inside the ‘sensor circuitry’, e.g. the detector current or other signals in the focal plane processor, can easily be monitored in simulation. Measurement of many of these signals in hardware is impossible. The simulation provides an environment where insight is obtained and understanding of the hardware is improved.

Often, faults and deficiencies observed in hardware in the laboratory, are traced by comparing simulation results with laboratory measurements. An example is the optimisation of noise performance in the sensor. The simulation model supplies the hardware developers with a realistic expected sensor background noise level. The three-dimensional noise analysis framework[35] is used as noise performance measurement tool. This predicted noise floor serves as a clear target for hardware noise reduction efforts.

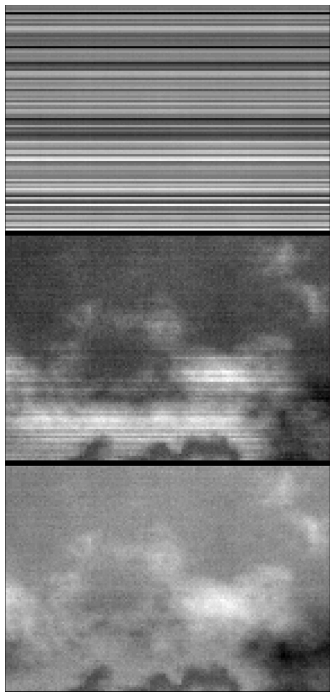

Figure 8. Cloudy sky sensor image before DCS and NUC (top), after DCS (middle) and after DCS and NUC (bottom).

7.1.3 Missile Seeker Dome Heating

The effect of the heated dome and heated, compressed air on the performance of an imaging sensor was studied in a closed loop supersonic missile flight simulation. This type of analysis is very difficult, if not impossible, in a real-world missile flight test. The dome temperature and its effect on the seeker performance was investigated for various mach numbers and ambient temperatures. During supersonic missile flight, the air in front of the dome is heated and compressed to such an extent that the carbon dioxide (CO_2) in the air becomes a significant source of infrared radiation in the mid IR. The radiation of heated, compressed air was measured in a pressure cell in the laboratory using a spectral radiometer. The measured data fitted the CO_2 band radiation model in Bernstein[36] and the model was used to predict dome heating flux.

The top left graph of Figure 9 shows the variation in dome and compressed air temperatures during simulated flight. The flux contribution of the radiating sources is shown in the bottom left graph. The scene and optics flux components of Equation 7 are negligibly small compared to the other three contributors. Note that initially, the radiation of the optics mounting is the main contributor, but as the dome temperature increases during flight, radiation from the dome becomes dominant. The increase in detector current at high mach numbers is shown in the top right graph. Due to the increase in dome and air temperature over the duration of a single scanned sensor image frame, a gradient develops across the image during scanner movement, shown in the bottom right picture in Figure 9. The influence of the hot dome on the sensor DCS control, image processing, detection and tracking algorithms was successfully optimised, using the closed loop simulation.

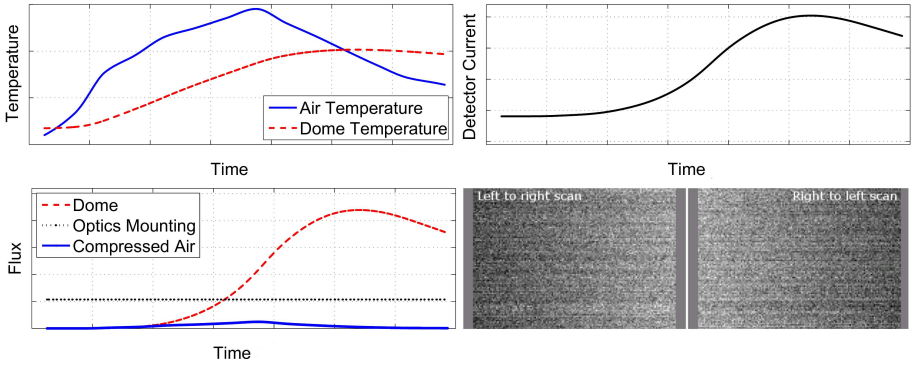

Figure 9. Sensor model results for a simulated supersonic missile flight.

7.1.4 Image Processing Algorithm Development

The most comprehensive application of OSSIM is in the development of image and information processing algorithms for an imaging air-to-air missile seeker. The detailed sensor model creates images that closely represent the actual hardware sensor images. The target detection, tracking and countermeasure rejection algorithms

are developed in a closed loop 6-degrees-of-freedom simulation, evaluated and optimised during thousands of simulated missile flights. The algorithms are evaluated under widely varied scenarios, background clutter conditions, flight conditions, target manoeuvres and countermeasure programs. Missile flight tests against real-world targets indicated that the algorithms performed exactly as observed during simulation. This observation can be considered a Turing-test, validating the simulation models and the process of algorithm development by simulation.[8,37]

7.1.5 Performance Prediction and Flight Test Preparation

The image simulation is used in various projects for performance prediction. In this application, the simulation is used to predict detection ranges, countermeasure performance, counter-countermeasure performance and missile tracking and guidance performance under high dynamics conditions.

The simulation is also used extensively for flight test preparation for a number of projects covering infrared missiles, automatic target recognition and countermeasure effectiveness evaluation applications. The planned flights, envisaged for the real-world trials, are programmed in the simulation approximating the test conditions; covering various atmospheric conditions as well as time of day or night. The simulation contributed significantly to flight test optimisation and risk reduction.

7.2 Infrared Scene Simulation in Missile Countermeasure Development

During peace-keeping operations South African Air Force (SAAF) aircraft experience a threat in the form of inexpensive Man Portable Air Defence (ManPAD) missiles. These missiles employ amplitude modulation (spin-scan) reticles or frequency modulation (conical scan) reticle seekers, with single element detectors. More recently developed missiles employ sensors with two spectral bands in order to to reject older-generation Magnesium Teflon Viton (MTV) flares. OSSIM is used to optimise aircraft countermeasures against these new ManPAD missiles. New flares are evaluated in simulation (and in field trials) and flare cocktails — carefully designed sequences of mixed flare types — are developed by extensive testing in the simulation.

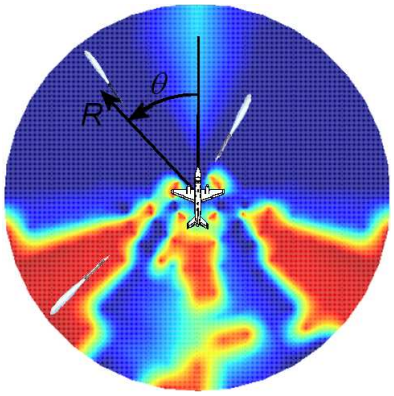

Figure 10. Aircraft vulnerability results.

In the simulation, the missile models implement algorithms that calculate the image on the reticle, then rotate or nutate the image across the reticle pattern, calculating the instantaneous detector current. The detector signal is processed according to the missile signal processing, and the missile is guided towards the aircraft, by iterating through the missile flight. Since missiles can be launched at an aircraft from any position on the ground, it is necessary to optimise the flare-dispensing direction relative to the range and approach of the attacking missile.

The effect of flare spectral signature, ejection direction and flare sequence timings are evaluated using thousands of simulated missile firings, by simulating missile launches from different aspect angles θ and ranges R from the aircraft. An example vulnerability result is shown in Figure 10. Each spot in the graph represents a missile launch from that location. If the countermeasure is effective in decoying the missile away from the aircraft, the miss distance is large (indicated by blue) and if the missile passes close to the aircraft, the aircraft is vulnerable (indicated by red). The objective is to maximise the blue zones and minimise the red zones. Once the strategy is optimised in simulation, it must be tested for validity in the real world. Invariably, some test point results will be at variance with the simulation results, requiring further model improvements and redesign of the procedures. After a number of such cycles, the procedures are then accepted as part of the SAAF standard operating procedures.

8. CONCLUSION

The three described simulation systems originated from very different needs, but share a common approach to the rendering of infrared images. The similarity in rendering is evident in comparing Equations 1, 2 and 4. All

three systems also employ heat balance equations to calculate thermal signatures. The developers of all three systems recognise the difficulty of modelling the complexity of the real physical world, nevertheless reaching a high level of radiometric fidelity in their respective systems.

DIRSIG's remote sensing legacy resulted in greater awareness of secondary atmospheric and environmental contributions to the signature. Furthermore, DIRSIG terrain models contain much detail. OSMOSIS' maritime countermeasure objective places a high premium on modelling the vessel construction details. OSSIM's missile development focus resulted in accurate spectral models of gaseous objects and a broad based infrastructure where the renderer is but one of the elements, albeit the most important element!

OSMOSIS choses to express model detail by increased number of facets/polygons, while DIRSIG and OSSIM add textures for finer detail. DIRSIG and OSSIM use texture maps for basic spatial properties (e.g. emissivity), but also to define material properties (e.g. material types in the terrain) or facet/polygon radiance.

Of the three simulation systems, DIRSIG has more powerful multimodal sensor options, being driven by diverse user needs and academic objectives. OSSIM's infrastructure supports a wider range of arbitrary platforms, but with more conventional optronic sensors. OSMOSIS appears to have a specialised niche focus (predicting maritime signatures) with appropriate attention to the relevant detail.

Given the common approach to rendering signatures, it would be interesting to develop a set of standardised test targets for simulation, much like CUBI for measurements. With such a set of standard targets, inter-laboratory comparisons would be an invaluable tool for validation.

In conclusion, it is evident that all three systems follow essentially the same rendering model, thereby cross-validating each other. Small differences in detail aspects provide opportunities for further convergent development.

ACKNOWLEDGMENTS

The authors wish to thank J.P. Delport, Pieter Goede, Paul Retief and Peet Smit who reviewed the paper.

REFERENCES

[1] "Digital imaging and remote sensing image generation (DIRSIG)." `http://www.dirsig.org/` (2010).
[2] Thermoanalytics, "RadThermIR." `http://www.thermoanalytics.com/products/radthermir/index.html` (2010).
[3] "ShipIR/NTCS." `http://www.wrdavis.com/NTCS_intro.html` (2010).
[4] "The OSMOSIS project." `http://www.osmosis-project.org/wordpress/` (2011).
[5] AIM-9X, "Sidewinder air-to-air missile," (2000).
[6] Novinky, "Raytheon's AIM-9X achieves initial operating capability with the U.S. Air Force," (2003).
[7] Schlesinger, S., "SCS technical committee on model credibility: Terminology for model credibility," *Simulation* **32**, 103104 (1979).
[8] Sargent, R. G., "Verification and validation of simulation models," in [*Proc 1998 Winter Simulation Conference*], Medeiros, D. J., ed., **1**, 121130 (1998).
[9] Knepell, P. L. and Arangno, D. C., [*Simulation Validation (A Confidence Assessment Methodology)*], IEEE Computer Society Press (1993).
[10] Irobi, I. S., S, I., Irobi, R., Andersson, J., and Wall, A., "Correctness criteria for models' validation - a philosophical perspective," tech. rep., Departmentof Computer science & Computer Engineering (IDT), Maalardalen University, P.O. Box 883 721 23, Vasteras, Sweden. (2001).
[11] Martis, M. S., "Validation of simulation based models: A theoretical outlook," *The Electronic Journal of Business Research Methods* **4**(1), 39–46 (2006).
[12] Willers, C. J. and Willers, M. S., "OSSIM: Optronics scene simulator white paper," Tech. Rep. 6700-PG-103400-01 Rev 3, Council for Scientific and Industrial Research (CSIR) (2011).
[13] Schott, J. R., [*Remote Sensing: The Image Chain Approach*], Oxford University Press (2007).
[14] "DIRSIG user's manual." `http://dirsig.org/documentation` (11 2006).

[15] Brown, S. D., Sanders, N. J., Goodenough, A. A., and Gartley, M., "Modeling space-based multispectral imaging systems with DIRSIG," in [*Algorithms and Technologies for Multispectral, Hyperspectral, and Ultraspectral Imagery XVII*], amd Paul E. Lewis, S. S. S., ed., **8048**, SPIE, SPIE (2011).
[16] Peterson, E. D., *Synthetic Landmine Scene Development and Validation in DIRSIG*, Master's thesis, B.S. Clarkson University (1998).
[17] Ward, J. T., *Realistic Texture in Simulated Thermal Infrared Imagery*, PhD thesis, Rochester Institute of Technology (2008).
[18] Schott, J. R., Raqueno, R., and Salvaggio, C., "Incorporation of a time-dependent thermodynamic model and a radiation propagation model into infrared three-dimensional synthetic image generation," *Optical Engineering* **31**(7), 1505–1516 (1992).
[19] Meyers, J. P., *Modeling Polarimetric Imaging using DIRSIG*, PhD thesis, Michigan Technological University (2002).
[20] Brown, S. D. and Schott, J. R., "Verification and validation studies of the DIRSIG data simulation model," tech. rep., Rochester Institute of Technology (2010).
[21] Lapierre, F. D., Archer, C., and Acheroy, M., "New research results and validation on real data of the OSMOSIS open-source infrared ship signature modeling software," in [*5th International IR Target, Background Modelling & Simulation (ITBMS) Workshop*], (2009).
[22] Dumont, R., Robert, T., Verdavaine, Y., Lapierre, F., Acheroy, M., and Marcel, J.-P., "SAFIR, a testbed for maritime simulations," in [*3rd International IR Target, Background Modelling & Simulation (ITBMS) Workshop*], (2007).
[23] Lapierre, F., Marcel, J.-P., and Acheroy, M., "Design of an infrared ship signature simulation software for general emissivity profiles," in [*2nd International IR Target, Background Modelling & Simulation (ITBMS) Workshop*], (2006).
[24] Dumont, R., "SAFIR, a software architecture for model interoperability," in [*3rd International IR Target, Background Modelling & Simulation (ITBMS) Workshop*], (2007).
[25] Simoneau, P., Caillault, K., Fauqueux, S., Huet, T., Krapez, J. C., Labarre, L., Malherbe, C., and Miesch, C., "MATISSE: version 1.4 and future developments," in [*Optics in Atmospheric Propagation and Adaptive Systems IX*], (2006).
[26] "The Python computer language." `http://www.python.org/` (2011).
[27] "SWIG." `http://www.swig.org/` (2011).
[28] Lapierre, F. D., Acheroy, M., Bushlin, Y., Lessin, A. D., and Reinov, A., "Validation of RadThermIR and OSMOSIS thermal software on the basis of the benchmark object CUBI," in [*5th International IR Target, Background Modelling & Simulation (ITBMS) Workshop*], (2009).
[29] Lessin, A., "CUBI forum." `http://www.iard.co.il/cubi/` (2011).
[30] MODTRAN, "MODTRAN atmospheric radiative transfer model." `http://www.modtran.org/` (2009).
[31] Zissis, G. J., ed., [*The Infrared and Electro-Optical Systems Handbook, Sources of Radiation*], vol. 1, SPIE (1993).
[32] Jacobs, P. A., [*Thermal Infrared Characterization of Ground Targets and Backgrounds*], vol. TT26 of *SPIE Tutorial Texts in Optical Engineering*, SPIE (1996).
[33] Balick, L. K., Scoggins, R. K., , and Link, L. E., "Inclusion of a simple vegetation layer in terrain temperature models for thermal infrared signature prediction," Tech. Rep. Miscellaneous paper EL-81-4, U.S. Army Engineer Waterways Experiment Station (1981).
[34] Monteith, J. L. and Unsworth, M., [*Principles of Environmental Physics*], Arnold, London (1995).
[35] D'Agostino, J. A. and Webb, C. M., "Three-dimensional analysis framework and measurement methodology for imaging system noise," in [*Infrared Imaging Systems: Design, Analysis, Modeling, and Testing II*], Holst, G. C., ed., **1488**, SPIE (1991).
[36] Bernstein, L. S., "Band model parameters for the 4.3μm band from 200 to 3000k - II. prediction, comparison to experiment, and application to plume emission-absorption calculations," *Journal of Quantitative Spectroscopy and Radiative Transfer* **23**, 169–185 (May 1979).
[37] Willers, C. J. and Wheeler, M. S., "The validation of models in an imaging infrared simulation," in [*IEEE International Microwave and Optoelectronics Conference (IMOC)*], IEEE (2007).